Available online at www.sciencedirect.com
ScienceDirect
Pattern Recognition 41 (2008) 367–377
PATTERN RECOGNITION
THE JOURNAL OF THE PATTERN RECOGNITION SOCIETY
www.elsevier.com/locate/pr

A multiscale directional operator and morphological tools for reconnecting broken ridges in fingerprint images

M.A. Oliveira, N.J. Leite*

Institute of Computing, State University of Campinas, Brazil

Received 1 July 2005; received in revised form 9 April 2007; accepted 23 May 2007

Abstract

In this paper, we introduce a multiscale operator which, together with some morphological tools, can be used to reconnect broken components of fingerprint images. This operator, which can be applied to both binary and gray-scale pictures, extracts the orientation field of an image by taking into account information parameters of sets of pixels in a given neighborhood and located in different directions. It has proved to be very robust to noise and outperforms the gradient- and directional mask-based methods, generally used for orientation field definition. Although we illustrate its application in the fingerprint domain, the approach described here can be easily extended to images whose components exhibit well-defined directional information.

Keywords: Fingerprints; Multiscale directional information; Mathematical morphology; Image enhancement

1. Introduction

Nowadays, there is an increasing emphasis on the privacy and security of personal information and, therefore, the importance of accurate personal identification systems has also increased. In order to satisfy these requirements, automatic fingerprint identification systems (AFISs) were created and became the most widely used biometric technology [1] mainly due to the following characteristics:

- *Universality*: everyone has it;
- *Permanence*: remains invariant over lifetime;
- *Collectability*: easy to be collected;
- *Distinctiveness*: it is sufficiently different from one person to another, even in cases of identical twins [2].

Most AFISs are based on minutiae matching [3–6]. *Minutiae* are local discontinuities in the fingerprint pattern. The most important ones are *ridge ending* and *ridge bifurcation*, illustrated in the center of the images in Fig. 1.

The performance of an AFIS relies essentially on the quality of the input images whose noise or contrast deficiency can produce false minutiae or hide valid ones. Even high-quality images can yield false minutiae. That is the case, for example, of a person having cuts or scars in the fingers which introduces spurious discontinuities of different sizes in the ridges.

Several approaches have been developed for fingerprint image enhancement [7] using, among others, Fourier transform [8,9], Wavelet transform [10], Gabor filters [5,11,12], etc., and for minutiae filtering applied to binary [13–16] or gray-scale images [17].

To improve the quality of the fingerprint images, we address here the specific problem of reconnecting broken ridges. To the best of our knowledge, this is the first work that deals with the spurious discontinuities of the ridges apart from the problem of improving contrast between ridges and fingerprint background. As one can see in the literature, most fingerprint image enhancement techniques embed both contrast improvement and ridge reconnection problems in a more general procedure [3,5,6,10,12,18–20]. Nevertheless, some few works explicitly mention aspects concerning broken ridges in their enhancement approach. In Ref. [10], for example, the authors introduce an initial step to reduce the number of false

* Corresponding author. Tel.: +55 19 3788 5873; fax: +55 19 3788 5887.
E-mail addresses: marcelo.oliveira@ic.unicamp.br (M.A. Oliveira), neucimar@ic.unicamp.br (N.J. Leite).

0031-3203/$30.00
doi:10.1016/j.patcog.2007.05.019

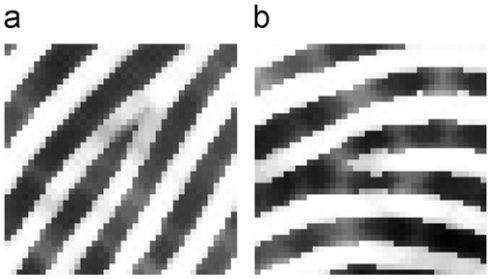

Fig. 1. Examples of minutiae: (a) ridge ending; (b) ridge bifurcation.

minutiae due to the presence of discontinuities. The method is based on a set of 16 pre-defined directional masks applied on the wavelet coefficients. The use of FFT on a set of pixels from a small region of the image, as in Ref. [9], allows a certain degree of reconnection of the broken ridges following the same FFT orientation. This FFT-based enhancement will be illustrated in Section 5.3 of this paper. In Ref. [18], the authors consider averages of the orientation field to deal with segments of broken ridges. The work in Ref. [3] takes into account these segments, in the context of minutiae detection, to filter out some spurious minutiae. However, as it will be shown here, a more specific way of treating broken ridges in fingerprint images allows a better consideration of other problems including, for instance, the variable length of such discontinuities. Naturally, this aspect is very important for increasing the performance of the whole reconnection step and, consequently, the quality of the resulting enhanced image.

Generally, in order to work with fingerprint images it is necessary to extract their orientation field representing local directions of the fingerprint ridges and valleys. To do so, several methods for estimating this information have been discussed in literature [21–24]. When the task consists in tracing flow lines, the methods that provide most accuracy are based on gradient computations [18,25–27], mainly due to their facility to deal with a large number of fixed possible directions [18]. This is not the case, for example, for the orientation field estimation based on Gabor filterbanks which, despite a better insensitivity to noise, is too computationally expensive for a large number of considered orientations and significantly influenced by the presence of creases and scars [28,29]. Indeed, many approaches for fingerprint image enhancement and ridge tracing consider a gradient-based orientation field information [3,5,18–20,27,30] or computations on sets of pixels defined by directional masks [6,10] as part of the method. Nevertheless, the presence of noise, smudges, broken or corrupted ridges in the input images may locally provide incorrect estimates. Approaches taking into account the orientation field model have also been discussed in literature. The method in Ref. [28] defines a polynomial model which depends on the correct identification of position and type of the fingerprint singular points (cores and deltas), as well as on the estimation of a set of parameters related to the polynomial coefficients.

This work proposes a method for reconnecting broken ridges based on morphological transformations and a multiscale neighborhood operator which estimates the orientation field of the fingerprint images. This operator characterizes the content of an image neighborhood, indicating the most likely orientation for each image pixel, by taking into account information parameters obtained from sets of points located in different directions. The maximum number of fixed directions in a given neighborhood is dictated by its size and, therefore, is a scale parameter for the whole process. As it will be illustrated elsewhere, this orientation field definition is less noise sensitive and yields a more accurate result than the typical approaches using gradient- and directional mask-based operators.

Although we focus this paper on the fingerprint domain, the method described here is quite general and can be easily extended to reconnect image components whose features can be associated with directional information. This is the case of applications concerning areas such as medicine, biometrics, metallurgy and geology.

The rest of this paper is organized as follows. Section 2 introduces basic concepts on Mathematical morphology and Section 3 defines an operator to extract directional information from images. We consider the problem of reconnecting fingerprint ridges in Section 4. Some experimental results and analyses are given in Section 5 followed by conclusions in Section 6.

2. Mathematical morphology

Our approach for reconnecting fingerprint ridges is based mainly on some mathematical morphology transformations [31–33], briefly discussed in this section, and on the multiscale directional operator introduced in Section 3.

2.1. Erosion and dilation

Erosion and dilation constitute the basis for more complex morphological operators and can be defined as follows.

Let $f : \mathbb{Z}^2 \mapsto \mathbb{Z}$ be a gray-scale image and $b : \mathbb{Z}^2 \mapsto \mathbb{Z}$ a plain structuring element. The gray-scale erosion of f by b, denoted by $f \ominus b$, is defined as

$$(f \ominus b)(x, y) = \min\{f(x + s, y + t) - b(s, t)\}, \quad (1)$$

where $(x + s, y + t) \in \mathscr{D}_f$, $(s, t) \in \mathscr{D}_b$ and $\mathscr{D}$ represents the discrete domain of the images.

The gray-scale dilation of f by b, denoted by $f \oplus b$, is defined as

$$(f \oplus b)(x, y) = \max\{f(x - s, y - t) + b(s, t)\}, \quad (2)$$

where $(x - s, y - t) \in \mathscr{D}_f$ and $(s, t) \in \mathscr{D}_b$.

As discussed in the next section, by iteratively applying erosion and dilation, one can eliminate image details, smaller than the structuring element, without affecting its global geometric features.

2.2. Closing and opening

Closing and opening are two examples of elementary combinations of erosion and dilation. Visually, closing smoothes

the contours, fills narrow gulfs and eliminates small holes. The gray-scale closing of f by b, denoted by $f \bullet b$, is defined as

$$(f \bullet b) = (f \oplus b) \ominus b. \tag{3}$$

On the other hand, opening smoothes contours, break narrow isthmuses and eliminates small islands. The gray-scale opening of f by b, denoted by $f \circ b$, is defined as

$$(f \circ b) = (f \ominus b) \oplus b. \tag{4}$$

2.3. Watersheds

The watershed is a very important morphological tool used in image segmentation and an intuitive definition of this transformation is given here. Formal definitions can be found, for instance, in Refs. [33–35].

Let f be a gray-scale image and $m_i(f)$ its regional minima (sets of pixels at a certain level l such that their external bounding pixels have a value strictly greater than l). Now, consider f as a topographic surface where the gray value of each pixel represents the altitude and each minimum $m_i(f)$ is pierced. We will flood this topographic surface by submerging it into a lake with a constant vertical speed. During the flooding process, two or more floods coming from different minima may merge. Every time it happens, we build a dam at the points where the floods would merge. At the end of the process, only the dams emerge. These dams define the watershed lines of the image f, segmenting the image in several basins $b_i(f)$. Each basin $b_i(f)$ contains one and only one minimum $m_i(f)$ and corresponds to the influence zone of this minimum.

3. The multiscale directional operator

This section presents a multiscale directional operator for estimating the orientation field of every pixel of an input image whose components exhibit well-defined directional information. Later, we illustrate the specific use of this operator in fingerprint image enhancement by considering, specifically, the broken ridge reconnection problem.

The following definitions are useful for the operator description. Let Γ be a sliding window of size $M \times N$ (usually, $M = N = (2l + 1)$, $l \in \mathbb{Z}^+$) of a digital image $f(\mathbf{x})$, $f : \mathbf{x} \in \mathbb{Z}^2 \mapsto f(\mathbf{x}) \in \mathbb{Z}$. Also, let D be the number of considered directions in Γ, and n the corresponding number of pixels in a given direction. In this work, we refer to these pixels as *test points*. Note that to represent all D directions in a two-dimensional grid, the number n of test points has a minimum bound, that is, for n test points, we can define up to $(2 \cdot n - 2)$ directions in a $n \times n$ neighborhood [33].

By considering the origin $(0, 0)$ of the image grid as it upper left corner, we can define the coordinates (x, y) of a test point, in a given direction α, as follows:

$$x = x_{center} + k \cdot \cos(\alpha),$$

$$y = y_{center} + k \cdot \sin(\alpha)$$

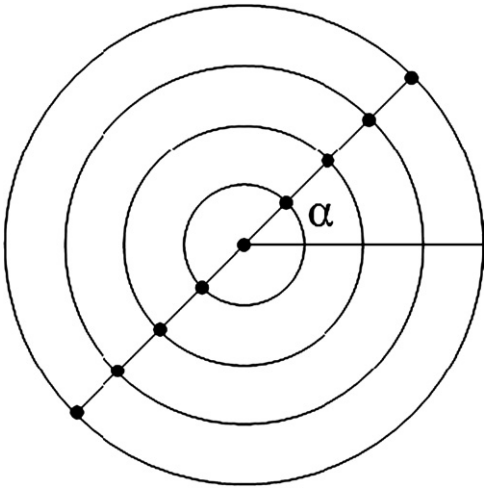

Fig. 2. Test points for $\alpha = 45°$ and $n = 9$.

for all k such that $-n/2 \leqslant k \leqslant n/2$. x_{center} and y_{center} are the coordinates of the point containing the sliding window Γ centered in this location. This procedure can be repeated for all D directions $(0, \ldots, D - 1)$ by changing the value of α accordingly $(\alpha = 0, 1 \cdot 180/D, 2 \cdot 180/D, \ldots, (D - 1) \cdot 180/D)$. Fig. 2 shows the test points for $\alpha = 45°$ and $n = 9$.

Now, let d_i^n be the set of the n test points in a given direction d_i. If we define the information to be retrieved from this set as a parameter characterized by any local descriptor (e.g., mean, standard deviation, moments of higher orders, morphological measures, etc.) and expressing features of this set, such as homogeneity, contrast, directionality, and so forth, our multiscale neighborhood operator can be described as follows:

(1) Set D to the number of directions to be considered and n to at least $(D + 2)/2$.
(2) Compute an information parameter (e.g., the standard deviation) on d_i^n for each of the D directions. In terms of implementation issues, we can store these data into an array $A[i]$, where $i \in \{0, 1, \ldots, D - 1\}$.
(3) The information associated with each direction d_i in Γ is compared with the one obtained from another direction d_j, $i \neq j$. For perpendicular directions, for example, the value of $A[i]$ is compared with $A[i + D/2]$, where $i \in \{0, 1, \ldots, D/2 - 1\}$, and $i + D/2$ is the corresponding perpendicular direction.
(4) The pair of directions d_i and d_j exhibiting the highest information contrast (e.g., $\max_i\{|A[i] - A[i + D/2]|\}$, for perpendicular directions), in a given pixel, defines a new image g as follows:

$$g(x, y) = s(d_i^n, d_j^n) = k, \quad k \in \{0, 1, \ldots, D - 1\}, \tag{5}$$

where function $s : \mathbb{R}^2 \mapsto \mathbb{Z}$ relates the values extracted from sets d_i^n and d_j^n and indicates the direction d_k in which a certain feature (e.g., homogeneity) is best defined. Image g can be seen as a directional image having values in the

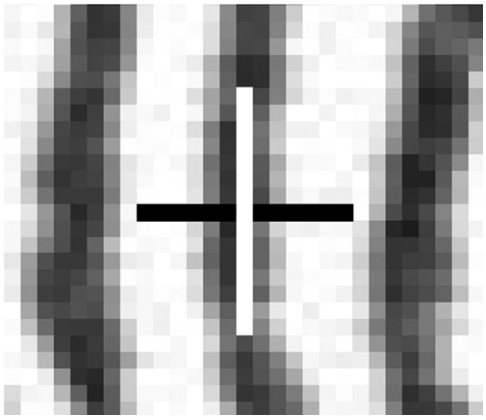

Fig. 3. Example of steps 3 and 4 of the proposed algorithm for a fingerprint image.

discrete range $[0, D-1]$, related to a contrast measure expressing the strength of the information parameter (e.g., the standard deviation) along a certain oriented direction.

Fig. 3 illustrates steps 3 and 4 of the above algorithm where the standard deviation is used to indicate homogeneity in a fingerprint image. In this figure, the vertical and horizontal bars crossing the center of a sliding window of size 15×15 correspond to the perpendicular directions presenting the highest standard deviation contrast at this position.

The next section considers the specific problem of reconnecting fingerprint ridges based on the pixel-wise orientation field information described above.

4. Reconnecting fingerprint ridges

The approach for reconnecting broken ridges consists mainly of the following steps, as shown in Fig. 4:

- *Orientation field estimation*: this step computes the most likely orientation for each pixel in the fingerprint image.
- *Image enhancement by watersheds*: the watershed transform gives the influence zone of all regional minima of the image. Note that in the binary case it defines the influence zone of each fingerprint ridge.
- *Definition of markers*: a subset of the watershed lines, representing regions of broken ridges, is obtained in this step.
- *Estimation of the distance between broken ridges*: the distance transform is applied to a set defined from the difference between two orientation field scales which results in an estimate of the distance between broken ridges.
- *Directional opening by markers*: to reconnect the broken components, a directional morphological opening is applied to the regions of the markers defined above, where the opening size parameter is based on the estimated distance between broken ridges.

Next, we describe with some details each of these steps.

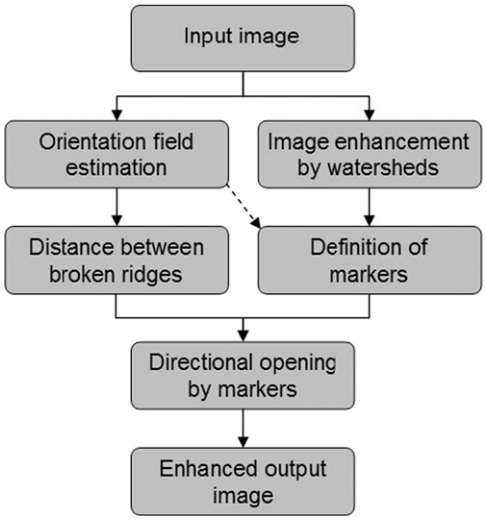

Fig. 4. General flowchart of the proposed method.

4.1. The orientation field estimation

In this section, we consider the operator described in Section 3 and its specific parameters to obtain the orientation field of fingerprint images. Note that local ridge directions are usually computed for a set of $W \times W$ nonoverlapping blocks of an image rather than for each pixel, as it is the case here.

For the information parameter, we use the *standard deviation* which expresses the homogeneity of each set d_i^n. In such a case, a pair of directions, i and $i+D/2$, exhibiting the highest contrast information defines the new directional image g as follows:

$$g(x,y) = \begin{cases} i & \text{if } \sigma(d_i^n) < \sigma(d_{i+D/2}^n), \\ i + \frac{D}{2} & \text{if } \sigma(d_i^n) > \sigma(d_{i+D/2}^n), \\ v & \text{otherwise,} \end{cases} \tag{6}$$

where the above function indicates the direction of the most homogeneous d^n set defined according to the standard deviation descriptor σ, and v is a special differentiable value representing the result of the function in a homogeneous region, i.e., with $\sigma(d_i^n)$ equal to $\sigma(d_{i+D/2}^n)$.

Fig. 5 shows an idealized 3D representation of a fingerprint. Intuitively, we can see that the standard deviation value along the ridges or valleys is smaller than the one computed in its perpendicular direction. Fig. 6 illustrates different scales, i.e., different number of test points and directions for the same fingerprint image and using the standard deviation as the descriptor of the homogeneity degree along the considered directions. Note that for a window Γ of size $2l+1$, we can have an "upscaling" (a more precise representation) of the directional information by at most a factor 4 as l increases by 1.

Note that although we focus our discussion on the orientation field estimation of a gray-scale fingerprint image, the operator introduced in Section 3 can be applied to any image (even binary, as we will see in Section 4.3) having components exhibiting well-defined directional information.

The approach described above defines a directional image whose pixels indicate the orientation of the image compo-

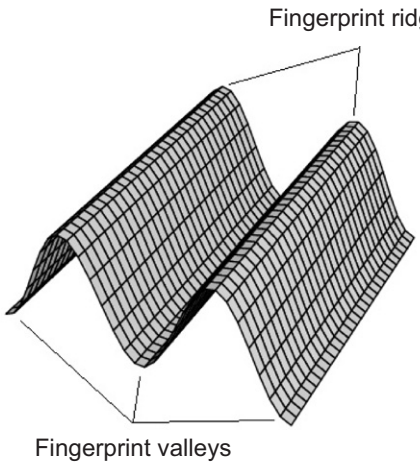

Fig. 5. Idealized 3D representation of a fingerprint.

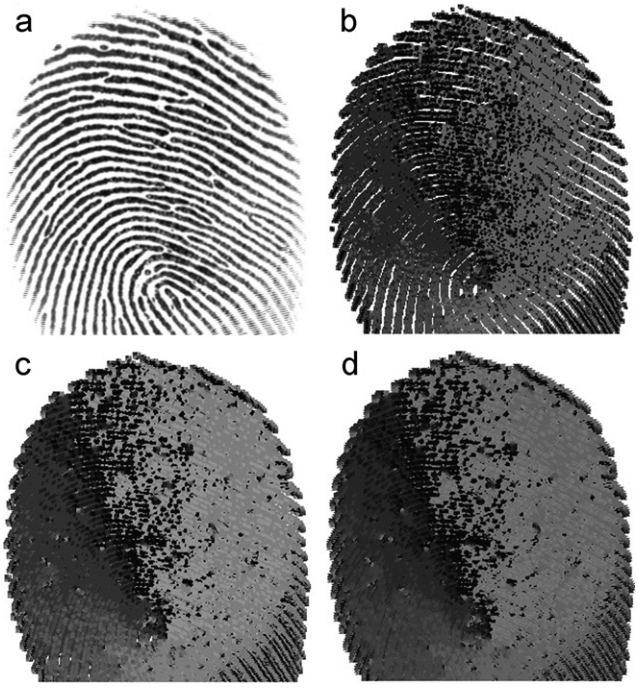

Fig. 6. Orientation fields with different scales for the same fingerprint image: (a) original fingerprint image; (b) orientation field for $D = 4$, $n = 3$, 4 gray levels; (c) orientation field for $D = 8$, $n = 5$, 8 gray levels; (d) orientation field for $D = 12$, $n = 7$, 12 gray levels.

nents with respect to the neighborhood Γ, the precision of this information being proportional to the number of considered directions D. Due to the discrete domain of the image and its limitations in accurately representing all the directions in a given neighborhood, some pixels may have locally uncorrelated values, thus yielding a noisy version of the directional information. A common solution to this problem consists in splitting the image into blocks of size $W \times W$ and replacing each pixel of a block by the direction exhibiting the highest frequency inside this block.

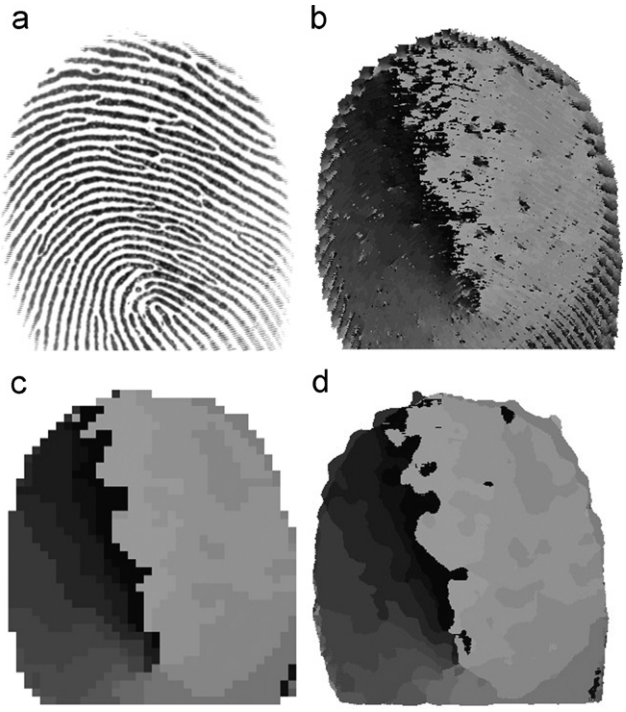

Fig. 7. Orientation field estimation for a fingerprint image ($D = 16$, $n = 15$). For the purpose of visualization, each direction in (b, c, d) is represented by a gray-scale value ranging from 0 to 150, in steps of 10, and defined in degrees as $f(x, y)/10 \cdot 11.25$: (a) original fingerprint image; (b) original orientation field image; (c) orientation field after a block-wise filtering; (d) orientation field after a pixel-wise filtering.

This block-wise approach is coarse since it hides image details and causes abrupt direction changes from one block to another. So, in order to obtain a finer orientation field information, we consider a pixel-wise approach in which a block of size $W \times W$ is centered at a given pixel and the direction exhibiting the highest frequency inside the block is attributed to this central pixel. From now on, we refer to the block used in our pixel-wise approach as a *smoothing window* Ω. Note that the size of this block, together with the size of the neighborhood Γ, constitutes a scale factor of the whole process. The block-wise and the pixel-wise filtering methods are illustrated in Figs. 7(c) and (d), respectively, for the original orientation field image in Fig. 7(b).

4.1.1. The orientation field of broken ridges

The algorithm described so far has proved to be very robust even in cases of fingerprint image problems involving noise, acquisition from dry or wet fingers, shadows from late fingerprints, etc. Nevertheless, in cases of components with large regions of broken ridges caused, for instance, by cuts or scars (see Fig. 8(a)), the detected orientations correspond to directions perpendicular to the actual ridge orientation. Thus, the regions associated with the disconnected ridges are represented in the directional image g by an abrupt change of orientation, as shown in Fig. 8(b). The use of this information, combined with the filtering operation by different smoothing windows Ω, will

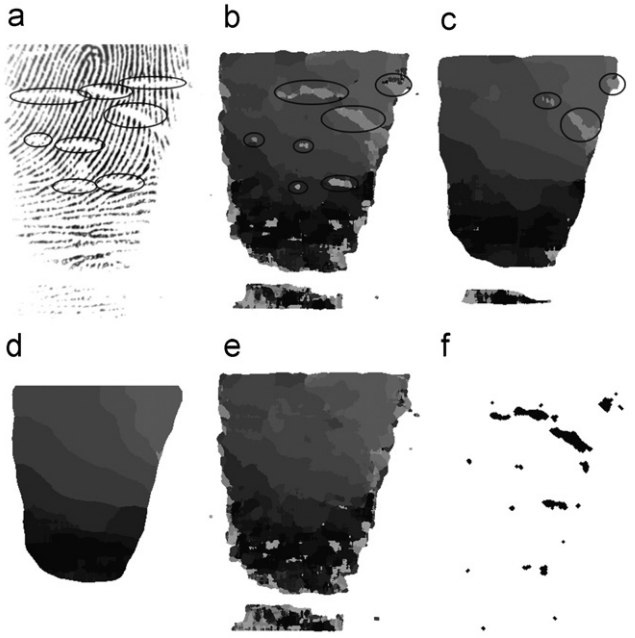

Fig. 8. Examples of different scales of a directional image and the orientation field rectification based on a coarser directional image. The highlighted areas show the broken ridges and the directions unproperly defined with respect to this coarser directional information (a directional image filtered by a large smoothing window): (a) original image with broken ridges; (b) orientation field filtered with a 15×15 smoothing window; (c) orientation field filtered with a 31×31 smoothing window; (d) orientation field filtered with a 45×45 smoothing window; (e) orientation field image with a 15×15 smoothing window after rectification; (f) set of rectified pixels given by the difference between (e) and (b).

be explored here to detect those pixels between disconnected ridges.

Indeed, as we will see next, the filtering of the directional image by a smoothing window of increasing size defines a multiscale representation of this image conveying useful information about the components connectivity. In a general way (see Fig. 8 for illustration), we have that a filtering of the directional image, by a small window Ω (Fig. 8(b)), yields a finer representation of the orientation field than the one obtained from larger windows Ω (Figs. 8(c) and (d)).

This multiple representation of the directional information can be used to define the regions between disconnected components of an image, as follows:

(1) Define two images g_s and g_l corresponding to the directional image g filtered with a small (Ω_s) and a large (Ω_l) smoothing window of sizes $(2s+1) \times (2s+1)$ and $(2l+1) \times (2l+1)$, respectively, where $s, l \in \{1, 2, \ldots, \min(M/2, N/2)\}$ and $s < l$. Image g_s is a finer smoothed version of the directional information, while g_l is a coarser version. Note that g corresponds to the finest representation of the directional image smoothed by a window Ω_s with $s = 0$.

(2) Rectify the finer representation of the directional image g, g_s, by taking into account the pixel-wise perpendicularity between images g_l and g_s as follows:

$$g'_s(x, y) = \begin{cases} g_l(x, y) & \text{if } g_l(x, y) \perp g_s(x, y), \\ g_s(x, y) & \text{otherwise.} \end{cases}$$

(3) Define a set X as the pixels of g_s updated by the above operation, that is,

$$(x, y) \in X \quad \text{if } g_s \neq g'_s, \ \ \forall (x, y) \in \mathscr{D}_{g_s}.$$

This set corresponds to the regions between broken ridges and will be used further in the reconnection procedure.

The above steps correct the finer directional information along the disconnected components of the original image by changing the value of the pixels not filtered at a finer scale and represented by a local change of orientation along the image components.

Fig. 8 illustrates these steps for a fingerprint image with some broken ridges. Fig. 8(b) shows the original orientation field of the image in Fig. 8(a), after a filtering process with a smoothing window Ω_s of size 15×15. A coarser scale of this information, defined by a filtering with a 45×45 smoothing window Ω_l, is shown in Fig. 8(d). Fig. 8(e) corresponds to the orientation field in Fig. 8(b) rectified according to step 2 above. The difference between the rectified orientation field (Fig. 8(e)) and its original finer version (Fig. 8(b)) determines the set X shown in Fig. 8(f), which represents the regions between the broken ridges. Note that the size of the smoothing window is based on a coarse estimate of the broken regions we want to detect. The larger this window the more significant are the regions obtained representing broken ridges in the original fingerprint images.

4.2. Image enhancement by watersheds

As stated in Section 2.3, the watershed algorithm constitutes a powerful morphological tool used for segmenting regions based on the set of image minima.

In a general way, the final result of the watershed transform applied to fingerprints should have the following characteristics:

- Ideally, each fingerprint ridge, considered here as the valleys of the original image, should define a basin surrounded by the corresponding watershed lines. Naturally, this is the case for binary images since for gray-scale ones a single ridge can have more than one minimum which, after the watershed transformation, relates one ridge to a set of k basins, $k \geqslant 1$.
- Ideally, the watershed lines should be exclusively defined in the regions between ridges (the regional maxima) or, in cases of disconnectedness, in the regions between broken ridges. However, since each ridge in the gray-scale case can have more than one regional minimum, the corresponding watershed lines may also cross the ridges perpendicularly with respect to their dominant direction.

Fig. 9(b) illustrates a fingerprint image segmentation by watersheds. In order to reconnect the broken ridges, we define

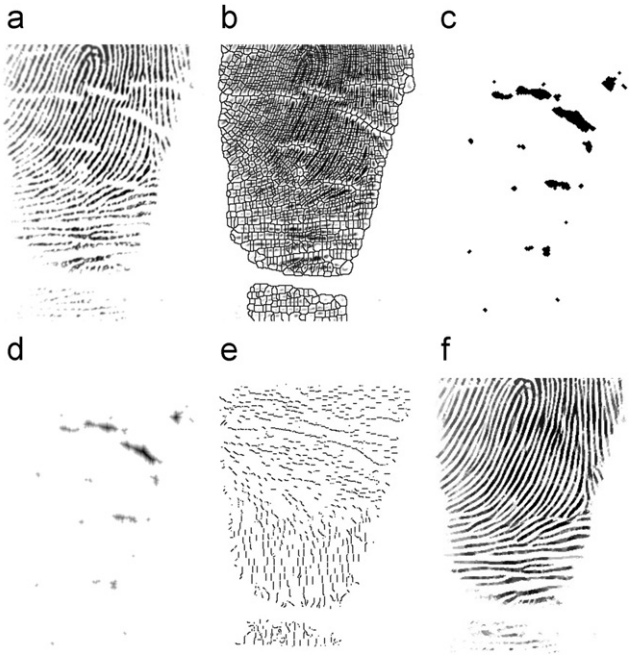

Fig. 9. Example of the operations used to reconnect the broken ridges of a fingerprint image: (a) original image; (b) watershed image; (c) set of pixels rectified at a finer scale; (d) distance transform image; (e) set of markers; (f) enhanced fingerprint image.

a set of markers based on the original image watershed lines, as explained next.

4.3. Definition of markers

Given the set of watershed lines of a fingerprint image, no matter if it is in the ideal segmentation case or not, we can combine this topographic information with the orientation field image (Section 4.1.1) to obtain a subset of watershed lines to be used as markers of the regions between broken ridges.

Let M be this subset and $L = \{l_1, l_2, \ldots, l_n\}$ the set of the original watershed lines. Informally, each line l_i is defined as the set of pixels between two bifurcations of the watershed lines (pixels whose connectivity number equals 2 for an 8-connected neighborhood [36]).

Now, consider the orientation field estimation (Section 4.1) of the watershed image. Note that, in such a case, we apply the algorithm described in Section 4.1 on a binary image. If the orientation of a line l_i of the set L is perpendicular to the ridge direction (a pixel-wise comparison between the orientation fields of the watershed and the original images provides this information), then it is very likely that l_i belongs to a region between broken ridges or between the regional minima of these ridges (see Fig. 9(b)). In such a case, l_i should be added to the set of markers M. Otherwise, if l_i has the same ridge direction, then this line is just defining the boundary between adjacent ridges and, therefore, should not be taken into account here.

The definition of the subset of the watersheds, representing markers for the regions between broken ridges, can be summarized by the following pseudocode:

$M = \emptyset$
For all line $l_i \in L$ **do**
  If l_i is perpendicular to the ridge direction **do**
    $M \leftarrow M \cup l_i$ /* Update the markers set */

4.4. Estimation of distances between broken ridges

The next step of our approach consists in estimating the distance between broken ridges in order to properly reconnect them.

To do so, we apply the distance transform [37] to the set X defined from the difference between the orientation field images at two different scales, as explained in Section 4.1.1. This set corresponds to pixels between broken ridges whose directional value was unproperly defined at a finer scale (orientation field image filtered by a small smoothing window Ω_s).

Fig. 9(d) shows the distance transform applied to the image in Fig. 9(c) representing the set of rectified pixels of the image in Fig. 8(b). Finally, the distance between the closest broken ridge to a given point of l_i, belonging to set X, can be defined as $(2 \cdot \mathrm{d}t + 1)$, where $\mathrm{d}t$ is the distance transform value at this point.

4.5. Directional opening by markers

The set M defined in Section 4.3 marks the regions considered in our last step which reconnects ridges and enhances the whole fingerprint image. This procedure can be accomplished by a morphological directional opening taking into account the markers l_i in set M, the distance transform of the components in set X, and the information at a certain scale of the orientation field image.

Shortly, the reconnection of the broken ridges is obtained by implementing, for each point of a marker l_i belonging to the set X, a morphological opening on a line segment of length $(2 \cdot \mathrm{d}t + 1)$ by a linear structuring element of the same size, centered at this point. The orientation of this opening corresponds to the ridge direction given by the orientation field image.

The same directional opening is defined for those markers l_i, belonging to regions between broken ridges, whose directional information was properly defined at a finer scale. Note that these regions are not included in the set X and, in such a case, the length of the considered linear structuring element should be small (e.g., 5) and proportional to the size of the window Ω_s.

Fig. 9 illustrates the main steps of our reconnection procedure for the original image in Fig. 9(a), and Figs. 10(e)–(h) show the final results of the method applied to several fingerprint images in Figs. 10(a)–(d). All these results were obtained by considering the following parameters: $D = 16$ directions, $n = 9$ test points and smoothing windows Ω_s and Ω_l of sizes 15×15 and 45×45, respectively.

Fig. 10. Other examples of our approach with $D=16$ directions, $n=9$ test points and smoothing windows Ω_s and Ω_l of sizes 15×15 and 45×45, respectively. (a, b, c, d) Original fingerprint images. (e, f, g, h) Enhanced images.

5. Experimental results

In this section, we carry out two different experiments with the purpose of illustrating some aspects of the proposed method and comparing the performance of our algorithm against others described in the literature. The first experiment considers our orientation field estimation approach (Section 4.1) and algorithms based mainly on the gradient information [3,18–20,38] or on two-dimensional masks corresponding to approximations of different directions [6,10]. The second experiment compares our entire approach with an enhancement technique based on the Fourier transform [9] which somehow also succeeds in reconnecting broken ridges.

For these comparisons, we restricted ourselves to a set of 200 fingerprint images whose results were compared quantitatively by a human operator. The fingerprint images used here were obtained from the FVC2002 (Fingerprint Verification Competition) databases [39].

5.1. Comparison criteria

Two criteria were used to compare the results quantitatively, namely, the *sensitivity* and the *specificity*, defined as

$$\text{Sensitivity} = 1 - \frac{\text{Number of not-corrected broken ridges}}{\text{Ground truth number of broken ridges}},$$

$$\text{Specificity} = 1 - \frac{\text{Number of miscorrected broken ridges}}{\text{Ground truth number of broken ridges}}.$$

To obtain these data, the original and the enhanced fingerprint images were analyzed manually in order to determine the ground truth number of broken ridges and the number of good corrections, miscorrections and missed corrections.

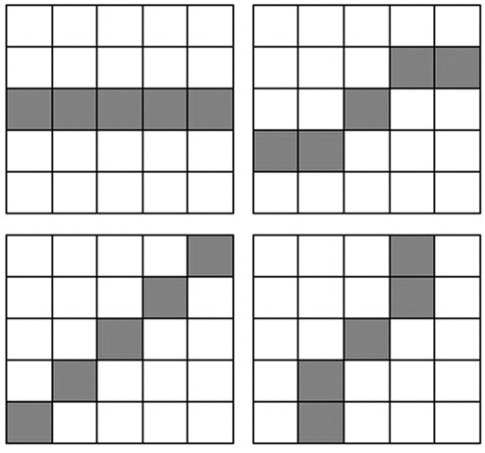

Fig. 11. Example of four orientations in 5×5 directional masks.

5.2. Orientation field comparison

In the first experiment, our orientation field estimation step is replaced with other algorithms described in the literature. The objective here is to compare the enhanced images produced by each of them, with respect to their accuracy in the broken ridges reconnection issue. The other steps of our approach remain unchanged.

To do so, we compare our approach with an algorithm based on the gradient information which estimates the orientation field according to the following equation [3,38]:

$$d(x,y) = \frac{1}{2}\tan^{-1}\frac{\sum_W 2G_xG_y}{\sum_W (G_x^2 - G_y^2)} + \frac{\pi}{2}, \tag{7}$$

Table 1
Comparison between orientation field estimation algorithms

Fingerprint	Gradient information		Eight directional masks		Our approach	
	Sensitivity (%)	Specificity (%)	Sensitivity (%)	Specificity (%)	Sensitivity (%)	Specificity (%)
10_7	69.2	100.0	73.1	100.0	100.0	100.0
38_7	36.4	100.0	36.4	100.0	90.9	100.0
Mean[a]	61.0	88.0	58.5	96.3	85.7	96.7

[a]Mean for a set of 200 images.

Fig. 12. Examples of fingerprint image 10_7 from FVC2002 database processed with different approaches: (a) original image; (b) gradient approach; (c) eight directional masks approach; (d) fourier approach; (e) our approach.

Fig. 13. Examples of fingerprint image 38_7 from FVC2002 database processed with different approaches: (a) original image; (b) gradient approach; (c) eight directional masks approach; (d) Fourier approach; (e) our approach.

where G_x and G_y are the gradient values for the x and y directions, respectively, and W is a neighborhood of arbitrary size around the pixel (x, y). This neighborhood is necessary to reduce noise. In such a case, the gradient information was obtained using the Sobel operator, a neighborhood size of 15×15, and the refinement step suggested in Ref. [3].

As another experimental analysis, we also compare our orientation field with another class of algorithms which considers the difference between the pixels mean values in different orientations represented by discrete directional masks [6,10]. The configuration in Fig. 11 illustrates four directions in 5×5 masks.

Here, we take into account 9×9 masks representing eight different directions for the orientation field image. Quantitatively, Table 1 shows the results comparing the gradient- and the directional mask-based orientation field with our approach, while Figs. 12 and 13 illustrate qualitative results for two different fingerprint images. We note the good performance of our method in terms of both sensitivity and specificity comparison criteria.

5.3. Fourier comparison

In the second experiment, our whole approach is compared with an enhancement technique based on the Fourier transform which, besides filtering the original fingerprint image, yields good broken ridge reconnection results.

Following the algorithm described in Ref. [9], the Fourier transform is applied to subregions of the original image represented by windows of 32×32 pixels. The ridges direction inside these windows is supposed to remain constant. Once the Fourier transform is computed for each window, the magnitude value is powered to a constant α and the following equations are applied:

$$Magnitude = \sqrt{Real[C(x, y)]^2 + Imag[C(x, y)]^2}, \tag{8}$$

$$Real[C(x, y)] = Real[C(x, y)] \cdot Magnitude^{\alpha}, \tag{9}$$

$$Imag[C(x, y)] = Imag[C(x, y)] \cdot Magnitude^{\alpha}, \tag{10}$$

Table 2
Comparison of the proposed method with an enhancement technique based on the Fourier transform

Fingerprint	Fourier transform		Our approach	
	Sensitivity (%)	Specificity (%)	Sensitivity (%)	Specificity (%)
10_7	80.8	100.0	100.0	100.0
38_7	30.3	100.0	90.9	100.0
Mean[a]	61.7	95.1	85.7	96.7

[a]Mean for a set of 200 images.

where $C(x, y)$ is the complex number calculated by the Fourier transform at location (x, y), and $Real[C(x, y)]$ and $Imag[C(x, y)]$ are its real and imaginary parts, respectively. Empirically, the authors suggest the value 1.4 for the constant α. After applying these equations, the inverse Fourier transform is calculated for each window, thus creating an enhanced fingerprint image.

The above procedure intensifies the image components having well-defined directions, in this case, the fingerprint ridges. Hence, for regions with broken ridges smaller than the considered window size, the method tries to fill in the gaps between the endpoints of the ridges, visually defining a lighter gray component reconnecting them (see Figs. 12(d) and 13(d)). A significant drawback of this approach is its possibility to break up bifurcations due to the lack of a well-defined direction in the corresponding region. Here, we did not measure the impact of this problem since we took mainly into account aspects concerned with the broken ridges reconnection.

Table 2 shows the comparison results between this enhancement technique and our proposed method. Once again, we note the good balance of our approach, in terms of the criteria described in Section 5.1, which indicates the excellent performance of the method when we consider both the high number of properly corrected components (sensitivity) and the few number of miscorrected broken ridges (specificity).

6. Conclusions

This work introduced a multiscale operator that extracts directional information from image components. This operator, which is less noise sensitive than the gradient- or directional mask-based methods, has proved to be very accurate in its pixel-wise representation and can be straightly applied to binary or gray-scale images. In terms of fingerprints, besides turning the minutiae filtering operations less time-consuming, the operator can be used as well to improve ridge following algorithms and minutiae extraction steps.

We also developed a morphological approach for reconnecting broken ridges of fingerprint images that can be easily extended to connect image components whose features can be described by directional information. This problem concerns many image processing applications in areas such as medicine, biometrics, metallurgy and geology.

As future works, we intend to consider the proposed multiscale operator in new problems including image segmentation and classification and improve the method performance through the use of adaptive neighborhoods, for instance, in regions presenting abrupt direction changes near the fingerprint singular points, such as cores and deltas.

Acknowledgments

The authors are grateful to Griaule and FAPESP for technical and financial support, respectively.

References

[1] D. Maltoni, D. Maio, A.K. Jain, S. Prabhakar, Handbook of Fingerprint Recognition, first ed., Springer, New York, 2003.
[2] A.K. Jain, S. Prabhakar, S. Pankanti, On the similarity of identical twin fingerprints, Pattern Recognition 35 (2002) 2653–2663.
[3] A. Jain, L. Hong, R. Bolle, On-line fingerprint verification, IEEE Trans. Pattern Anal. Mach. Intell. 19 (4) (1997) 302–313.
[4] D. Maio, D. Maltoni, Direct gray-scale minutiae detection in fingerprints, IEEE Trans. Pattern Anal. Mach. Intell. 19 (1) (1997) 27–39.
[5] L. Hong, Y. Wan, A. Jain, Fingerprint image enhancement: algorithm and performance evaluation, IEEE Trans. Pattern Anal. Mach. Intell. 20 (8) (1998) 777–789.
[6] Y. He, J. Tian, X. Luo, T. Zhang, Image enhancement and minutiae matching in fingerprint verification, Pattern Recognition Lett. 24 (2003).
[7] A.K. Jain, S. Pankanti, S. Prabhakar, A. Ross, Recent advances in fingerprint verification, Lect. Notes Comput. Sci. 2091 (2001) 182–191.
[8] B.G. Sherlock, D.M. Monro, K. Millard, Fingerprint enhancement by directional fourier filtering, IEEE Proceedings in Visual Image Signal Processing, vol. 141(2), April 1994, pp. 87–94.
[9] A.J. Willis, L. Myers, A cost-effective fingerprint recognition system for use with low-quality prints and damaged fingertips, Pattern Recognition 34 (2001) 255–270.
[10] C. Hsieh, E. Lai, Y. Wang, An effective algorithm for fingerprint image enhancement based on wavelet transform, Pattern Recognition 36 (2003) 303–312.
[11] S. Greenberg, M. Aladjem, D. Kogan, Fingerprint image enhancement using filtering techniques, Real Time Imaging 8 (2002) 227–236.
[12] J. Yang, L. Liu, T. Jiang, Y. Fan, A modified Gabor filter design method for fingerprint image enhancement, Pattern Recognition Lett. 24 (2003) 1805–1817.
[13] Q. Xiao, H. Raafat, Combining statistical and structural information for fingerprint image processing classification and identification, in: Pattern Recognition: Architectures, Algorithms and Applications, World Scientific, River Edge, NJ, 1991, pp. 335–354.
[14] D.C.D. Hung, Enhancement and feature purification of fingerprint images, Pattern Recognition 26 (11) (1993) 1661–1671.
[15] A. Farina, Z.M. Kovacs-Vajna, A. Leone, Fingerprint minutiae extraction from skeletonized binary images, Pattern Recognition 32 (5) (1999) 877–889.
[16] B. Bhanu, M. Boshra, X. Tan, Logical templates for feature extraction in fingerprint images, Proceedings of the International Conference on Pattern Recognition (15th), vol. 2, 2000, pp. 850–854.
[17] D. Maio, D. Maltoni, Neural network based minutia filtering in fingerprints, Proceedings of the World Conference on Systems Cybernetics and Informatics, vol. 4, 1998, pp. 1654–1658.
[18] A.M. Bazen, S.H. Gerez, Systematic methods for the computation of the directional fields and singular points fingerprints, IEEE Trans. Pattern Anal. Mach. Intell. 24 (7) (2002) 905–919.
[19] A.M. Tahmasebi, S. Kasaei, A novel adaptive approach to fingerprint enhancement filter design, Signal Process. Image Commun. 17 (2002) 849–855.
[20] Q. Zhang, K. Huang, H. Yan, Fingerprint classification based on extraction and analysis of singularities and pseudoridges, Pattern Recognition 37 (11) (2004) 2233–2243.

[21] K. Karu, A.K. Jain, Fingerprint classification, Pattern Recognition 29 (3) (1996) 389–404.
[22] C.L. Wilson, G.T. Candela, C.I. Wilson, Neural network fingerprint classification, J. Artif. Neural Networks 1 (2) (1994) 203–228.
[23] L. O'Gorman, J.V. Nickerson, An approach to fingerprint filter design, Pattern Recognition 22 (1) (1989) 29–38.
[24] M. Kawagoe, A. Tojo, Fingerprint pattern classification, Pattern Recognition 17 (3) (1984) 295–303.
[25] A.R. Rao, R.C. Jain, Computerized flow field analysis: oriented texture fields, IEEE Trans. Pattern Anal. Mach. Intell. 14 (7) (1992) 693–709.
[26] M. Kass, A. Witkin, Analyzing oriented patterns, Comput. Vision Graphics Image Process. 37 (3) (1987) 362–385.
[27] N. Ratha, S. Chen, A. Jain, Adaptive flow orientation-based feature extraction in fingerprint images, Pattern Recognition 28 (1995) 1657–1672.
[28] J. Gu, J. Zhou, D. Zhang, A combination model for orientation field of fingerprints, Pattern Recognition 37 (2004) 543–553.
[29] A.K. Jain, S. Prabhakar, S. Pankanti, Filterbank-based fingerprint matching, IEEE Trans. Image Process. 9 (5) (2000) 846–859.
[30] A.K. Jain, L. Hong, S. Pankanti, R. Bolle, An identity-authentication system using fingerprints, Proc. IEEE 85 (9) (1997) 1365–1388.
[31] J. Serra, Image Analysis and Mathematical Morphology, Academic Press, London, 1982.
[32] J. Serra, Image Analysis and Mathematical Morphology—Volume 2: Theoretical Advances, Academic Press, London, 1988.
[33] P. Soille, Morphological Image Analysis: Principles and Applications, Springer, Berlin, 1999.
[34] S. Beucher, S.F. Meyer, in: E. Dougherty (Ed.), The Morphological Approach to Segmentation: The Watershed Transformation, Marcel Decker Inc., New York, 1992.
[35] L. Vincent, P. Soille, Watersheds in digital spaces: an efficient algorithm based on immersion simulations, IEEE Trans. Pattern Anal. Mach. Intell. 13 (6) (1991) 583–598.
[36] S. Yokoi, et al., An analysis of topological features at digitized binary pictures using local features, Comput. Graphics Image Process. 4 (1975) 63–73.
[37] A. Rosenfeld, A.C. Kak, Digital Picture Processing, vols. I and II, Academic Press, Orlando, FL, 1982.
[38] A. Rao, A Taxonomy for Texture Description and Identification, Springer, New York, NY, 1990.
[39] FVC2002 Fingerprint Verification Competition. ⟨http://bias.csr.unibo.it/fvc2002/⟩.